Visualization of Lipid Membrane Reorganization Induced by a Pore-Forming Toxin Using High-Speed Atomic Force Microscopy

Neval Yilmaz[†] and Toshihide Kobayashi[*,†,‡]

[†]Lipid Biology Laboratory, RIKEN, Wako, Saitama 351-0198, Japan and [‡]INSERM U106-Université Lyon1, 69621 Villeurbanne, France

ABSTRACT We examined the effect of a sphingomyelin (SM)-binding pore-forming toxin (PFT), lysenin, on the dynamics of a phase-separated membrane of SM, where SM formed liquid-ordered (Lo) domains with cholesterol (Chol) within a phosphatidylcholine-rich liquid-disordered (Ld) phase. We visualized the lysenin-induced membrane reorganization using high-speed atomic force microscope (HS-AFM). Lysenin oligomerized on the SM-rich Lo domain and simultaneously its oligomers assembled into a hexagonal close-packed (hcp) structure. The phase boundary was stable during the assembling of lysenin on the SM-rich domain, indicating that lysenin did not affect the line tension between Lo and Ld phases. After the full coverage of the SM-rich domain by oligomers, their hcp assembly gradually expanded into the Ld phase and eventually covered the entire membrane. Our results suggest that pore formation, *i.e.*, insertion of lysenin into the membrane in its oligomeric state, induced the exclusion of SM and Chol from the SM-rich domain, which was followed by further binding and oligomerization of lysenin.

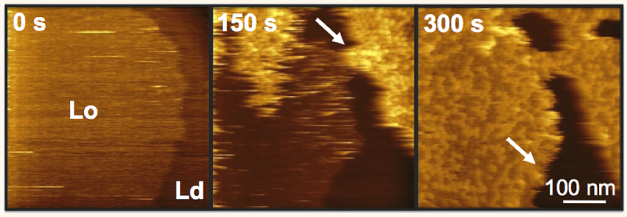

KEYWORDS: high-speed atomic force microscopy · phase mixing · sphingomyelin · lysenin · oligomer

Accumulating evidence indicates the importance of heterogeneous distribution of membrane lipids in a number of physiological phenomena as diverse as signal transduction to membrane traffic.[1−4] Especially, the assembly and dynamics of raft-like liquid-ordered (Lo) domains, enriched with sphingolipids and cholesterol (Chol), in liquid-disordered (Ld) membranes attract a lot of attention.[5−8] Several proteins are reported to reorganize the model membranes having both Lo and Ld phases by their insertion into the Ld phase and/or binding to the Lo/Ld phase boundary.[9−13] Ros *et al.*[12] shows that sticholysin, a sphingomyelin (SM)-binding pore-forming toxin from the actinoporin family, inserts into the SM-poor Ld phase and induces phase mixing by reducing the line tension between Lo and Ld phases. It is hypothesized that the decrease in line tension is caused by sticholysin localized at the phase boundary. Despite being an SM-binding protein, sticholysin does not prefer the SM-rich Lo phase. Another protein from the actinoporin family, equinatoxin II (EqtII), which has a very similar 3D structure to that of sticholysin,[14−16] also binds SM. Similarly, it accumulates in the Ld phase after localizing at the phase boundary.[13] Recent results indicate that EqtII binds SM when it is dispersed in the membrane, irrespective of the lipid phase.[17]

Lysenin is a 297-amino acid pore-forming toxin that specifically binds SM.[18,19] Its 3D structure[20] is different from those of sticholysin and EqtII. Unlike sticholysin and EqtII, lysenin exclusively binds the clustered SM.[21,17] We were interested in whether lysenin, an Lo-binding protein, would induce phase mixing as observed for sticholysin, an Ld-binding protein. Therefore, we followed the lysenin-induced changes in a phase-separated membrane of SM using high-speed atomic force microscopy (HS-AFM). Previously, we employed the same technique to visualize the assembling of lysenin on the SM/Chol membrane, exhibiting Lo phase, and revealed the stable hexagonal close-packed (hcp) assembly of

* Address correspondence to kobayasi@riken.jp.

Received for review February 13, 2015 and accepted July 29, 2015.

Published online July 29, 2015
10.1021/acsnano.5b01041

lysenin oligomers.[22] In case of the phase-separated membrane, lysenin first assembled on the SM-rich Lo phase and finally covered the entire membrane with its oligomers. Our results indicate that lysenin induces phase mixing in an oligomerization-dependent manner, a mechanism different from that of sticholysin. We infer that lysenin oligomers exclude SM and Chol from the Lo domain and thus the hcp assembly of oligomers can expand into the Ld phase, leading to a homogeneous morphology.

RESULTS

Assembling of Lysenin on SM/Chol/DOPC Membrane. We followed the oligomerization of lysenin on SM/Chol/DOPC (2:1:2) bilayer. The SM/Chol/DOPC bilayer segregated into the SM-rich higher phase and the DOPC-rich lower phase. The preferential partition of Chol in SM-rich domains was demonstrated for the SM/Chol/egg PC membrane.[23] In the presence of Chol, the SM-rich domains exhibit liquid-ordered phase, whereas DOPC-rich phase is liquid disordered.[24,25] Therefore, the SM-rich higher phase of the model membrane used in this study should be liquid ordered. The AFM image for the phase-separated bilayer on mica surface is shown in Figure 1A with the height profiles. The darkest region corresponds to the mica surface. The height profiles along the white and black lines indicate the vertical distances from the mica surface and the DOPC-rich phase, respectively.

Figure 1B and Movies 1A,B show the binding of lysenin to the SM-rich domain and the full coverage of this domain with an hcp structure as previously observed for the SM/Chol (1:1) bilayer.[22] The "0 s" in Figure 1B indicates an arbitrary time before the start of oligomerization. At 0 s, there were no detectable oligomers of lysenin in the scanned area. The spike-like features denote the rapidly diffusing lysenin monomers or oligomers. At 30 s, a single oligomer appeared on the SM-rich domain as a round bright feature (indicated by the arrow). The domain boundary was initially almost round and stable (see also Figure S1). However, during the formation of lysenin oligomers it showed slight fluctuations, which can be discerned at 120 s. At the same time, an hcp assembly (marked by the asterisk) appeared. At 150 s, the SM-rich domain and the hcp assembly, which had formed on another SM-rich domain, started to coalesce through a bridge-like structure (pointed out by the arrow). The arrows at 180 and 210 s indicate the growth of the hcp assembly toward the domain boundary. Interestingly, oligomer formation did not start at the boundary despite the line energy, favoring the adsorption of surfactants and proteins.[26,27] The same phenomenon was observed for two more experimental sets conducted under the same conditions. At 240 s, the SM-rich domain was fully covered with the hcp assembly of oligomers. At 300 s, this assembly showed a slight broadening (marked by the arrow). During the oligomerization of lysenin on

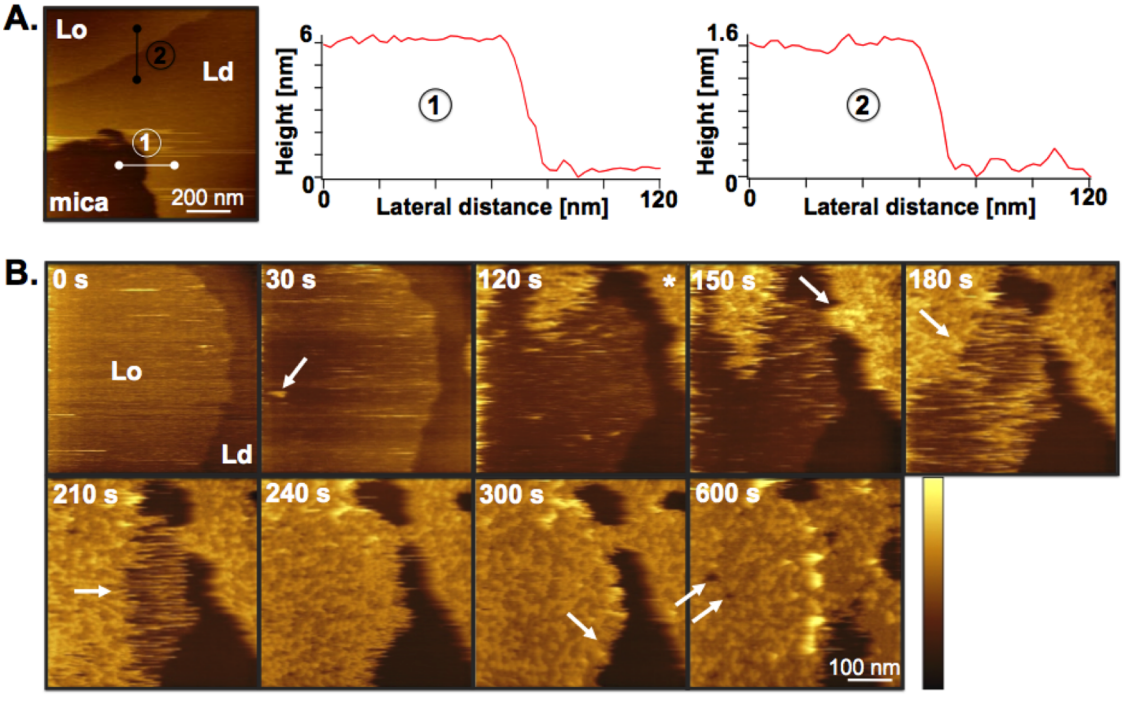

Figure 1. (A) AFM image of SM/Chol/DOPC (2:1:2) bilayer on mica and the corresponding height profiles. (B) Assembling of lysenin on SM/Chol/DOPC (2:1:2) membrane. The arrows show the single oligomer (30 s), bridging between two domains (150 s), growth direction of the hcp assembly (180 s, 210 s), broadening of the SM-rich domain (300 s), and appearance of darker regions within the hcp assembly (600 s). The asterisk at 120 s marks the hcp assembly on another SM-rich domain. The color bar indicates the *Z*-range between 0 (darkest) to Z_{max} (brightest); Z_{max} = 15 nm (0 s, 30 s), 20 nm (120 s, 150 s), 25 nm (180 s, 210 s), 28 nm (240 s, 300 s), 30 nm (600 s).

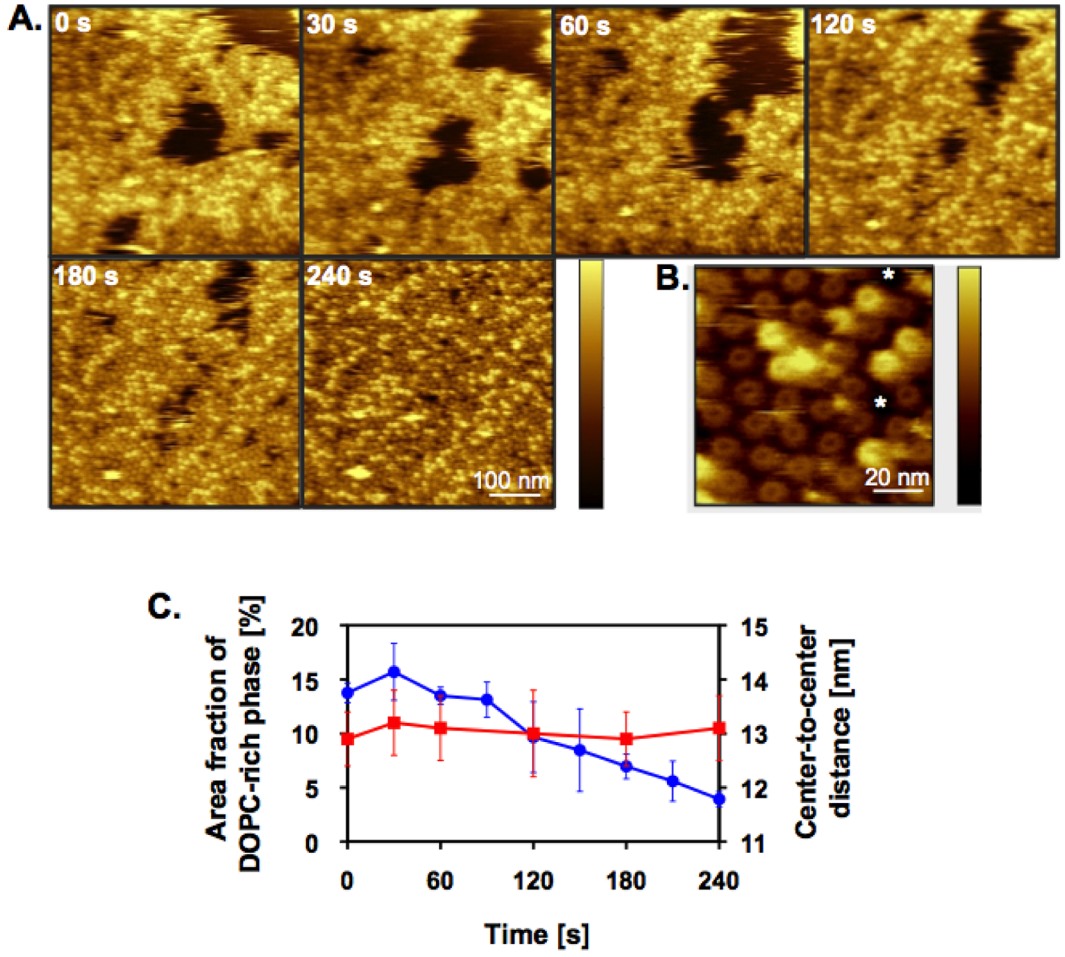

Figure 2. (A) Reorganization of SM/Chol/DOPC (2:1:2) membrane during assembling of lysenin. (B) The stabilized hcp assembly of lysenin oligomers. The asterisks mark the defects within the hcp assembly. The color bar indicates the *Z*-range between 0 (darkest) to Z_{max} (brightest); Z_{max} (A) = 17 nm (0 s, 30 s), 16 nm (60 s), 14 nm (120 s, 180 s), 10 nm (240 s), and Z_{max} (B) = 7 nm. (C) The time-dependent change in the area fraction of the DOPC-rich phase (in blue) and the center-to-center distance between oligomers (in red).

the SM-rich domain, we did not observe any oligomers in the DOPC-rich phase. After the SM-rich domain was fully covered with oligomers, the hcp assembly continued growing by the oligomerization of lysenin beyond the domain boundary (600 s). Simultaneously, darker regions appeared within the hcp assembly. Some of these regions are shown by the arrows at 600 s.

Membrane Dynamics during Assembling of Lysenin. The formation and reclosing of the darker regions during the completion of the hcp assembly are shown in Figure 2A and Movie 2. From the height images, these regions are judged to be the DOPC-rich phase. The change in the local membrane composition was reversible and took place by the lateral diffusion of small groups of oligomers. We followed the oligomer dynamics at a smaller scan size (Movie 3) and could visualize the lateral diffusion of an individual oligomer. The motion of an oligomer between the two edges of the hcp assembly, denoting the diffusion of a small cluster of SM through the DOPC-rich phase, is indicated by the arrows in Figure 3. As a result of the continuous formation of oligomers and their rearrangement on the membrane, the DOPC-rich phase shrank during incubation (Figure 2A). Despite the decrease in the area of the DOPC-rich phase, the center-to-center distance between the oligomers within the hcp assembly did not change over time (Figure 2C). With the use of FFT analysis, the neighboring distance was determined to be around 13 nm. This value agrees well with those calculated for the hcp assembly of lysenin oligomers on SM/Chol bilayer.[22] Figure 2B shows the final morphology of the membrane, almost fully covered with ring-like oligomers of lysenin, at a smaller scan size. The stable hcp assembly had some defects, which might be the confined DOPC (indicated by the asterisks).

Despite the fast reorganization of the membrane, most parts of the hcp assembly surrounding the DOPC-rich phase were stable over time intervals, such as 10 s (Figure 4). The images in Figures 4A,B belong to two different sets of experiments conducted under the same conditions. We chose the brighter (taller) oligomers as markers to judge the stability of the hcp assembly.

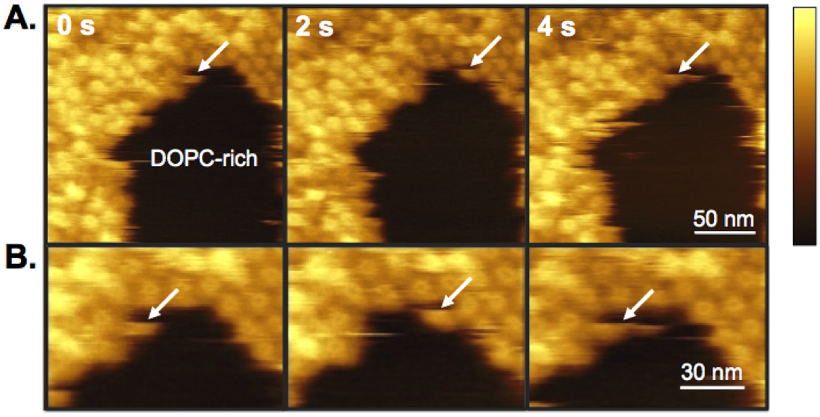

Figure 3. Motion of a single oligomer between the edges of the hcp assembly during membrane reorganization. The arrows point out the position of the oligomer at a time interval of 2 s. The areas showing the motion of the oligomer in (A) were enlarged in (B). The color bar indicates the *Z*-range between 0 (darkest) to Z_{max} (brightest); Z_{max} (A) = 18 nm.

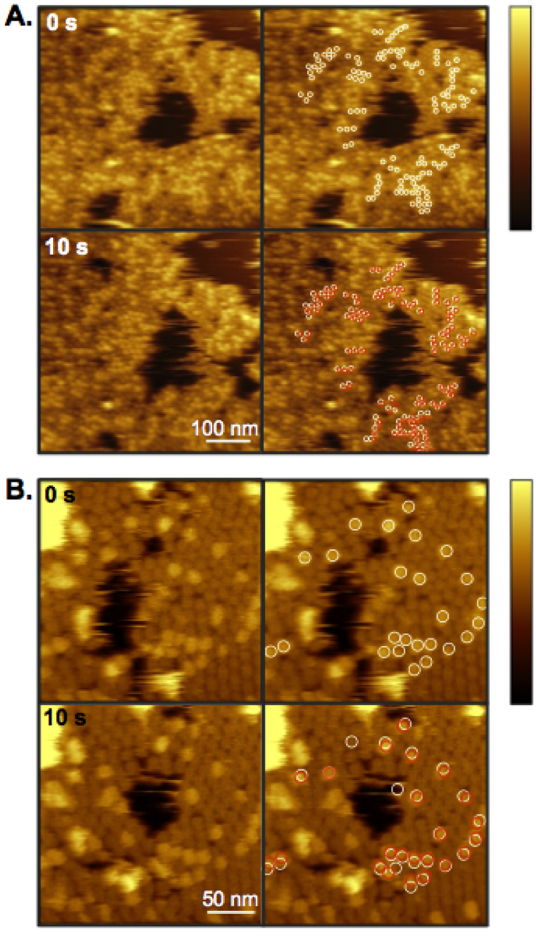

Figure 4. Stable hcp assemblies of lysenin oligomers during membrane reorganization. The images in (A) and (B) belong to two different experimental sets conducted under the same conditions. Some of the brighter oligomers in the images to the right are circled in white and red to indicate their positions at 0 and 10 s, respectively. The color bar indicates the *Z*-range between 0 (darkest) to Z_{max} (brightest); Z_{max} (A, B) = 20 nm.

Some of the brighter oligomers in the hcp assembly around the DOPC-rich phase are marked by white (0 s) and red (10 s) circles. In both experimental sets, the brighter oligomers have similar positions at 0 and 10 s.

Change in Membrane Area with Lysenin Assembly. We followed the change in the membrane area during the formation of the hcp assembly (Figure 5, Movie 4, and Movies 5A,B). In Figure 5A, the DOPC-rich region of the membrane was suddenly disrupted upon completion of the hcp assembly. During oligomerization of lysenin, the membrane area on which the hcp assembly formed gradually expanded until the disruption of the membrane (Figure S2). This result implies the shrinkage in the total membrane area. In Figure 5B, on the contrary, the membrane edge was not affected by the lysenin assembly. The blue and red arrows in Figure 5B point out the oligomerization direction after the formation of the hcp assembly on the SM-rich domain.

Oligomer Height Measured during Membrane Reorganization. We observed both low and tall oligomers during assembling of lysenin as well as after the formation of a stable hcp assembly. We measured the oligomer height during assembling of lysenin with respect to the DOPC-rich phase. The histogram in Figure 6 shows the oligomer height distribution with maxima at about 9.6 and 12.9 nm for low and tall oligomers, respectively. These height values correspond to the sum of the oligomer height and the height difference between SM-rich and DOPC-rich phases. The height difference between two phases before the start of oligomerization was approximately 1.5 to 2 nm. On the basis of this value, we calculated the height of low and tall oligomers to be around 8 and 11 nm, respectively. The oligomer height did not change during assembling of lysenin.

DISCUSSION

Previously, Ros *et al.*[12] showed that SM-binding pore-forming toxin, sticholysin, induces phase mixing in SM/Chol/DOPC (1:1:1) bilayer. It was speculated that the preferential binding of sticholysin to the phase boundary promoted a reduction in line tension between Lo and Ld phases and led to the domain

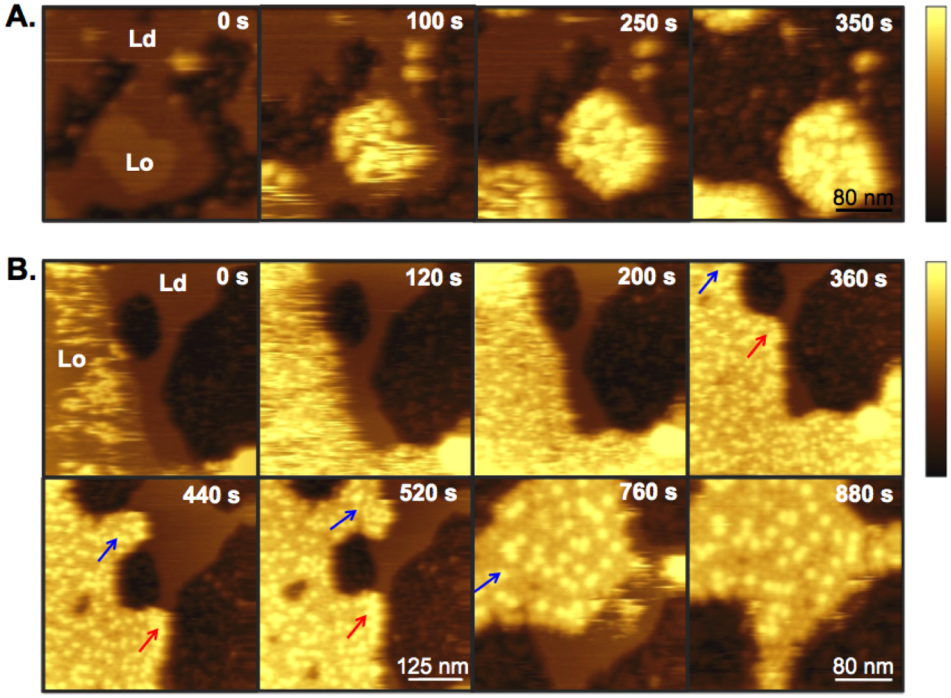

Figure 5. Effect of lysenin assembly on the membrane area. The images in (A) show the shrinkage in the membrane area, whereas those in (B) exhibit a stable membrane edge. The red and blue arrows in (B) denote the expansion of the hcp assembly of lysenin oligomers. The color bar indicates the *Z*-range between 0 (darkest) to Z_{max} (brightest); Z_{max} (A, B) = 20 nm.

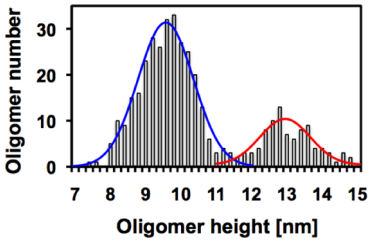

Figure 6. Histogram showing the height distribution for the low and tall oligomers with respect to the DOPC-rich phase. The heights of the low and tall oligomers were determined to be 9.6 ± 0.8 and 12.9 ± 0.7 by fitting the histogram with the Gaussian function. Gaussian curves for the low and tall oligomers are depicted in blue and red, respectively.

coalescence. Unfortunately, oligomeric assemblies of sticholysin could not be resolved in the same study. We followed the assembly of lysenin and membrane reorganization at a concentration of 1.5 μM, which is 6 times higher than that of sticholysin (0.25 μM) in Ros *et al.*[12] At 1.5 μM, we could visualize the hcp assembly of lysenin oligomers on the SM/Chol/DOPC (2:1:2) membrane. Different from sticholysin,[12] lysenin did not induce any significant change in the phase boundary during its binding and oligomerization on the SM-rich domain (Figure 1 from 0 to 240 s). This might imply the weak binding of lysenin to the domain boundary.

Additionally, the stability of the domain boundary might indicate that the increase in lateral pressure in the SM-rich domain after binding of lysenin to SM was not high enough to reduce the line tension and/or it was compensated by the high area compressibility in the presence of Chol.[28,29] It is highly possible that lysenin in the monomeric state did not insert into the membrane, and accordingly, binding of lysenin did not induce any changes in the lateral pressure and the phase boundary. On the other hand, as the number of oligomers on the SM-rich domain increases, the effect of lateral pressure should be more pronounced and the membrane should expand due to the available mica area. However, we observed either a shrinkage in the membrane area (Figure 5A) or a stable membrane edge (Figure 5B). The shrinkage in the membrane area in Figure 5A can be attributed to the increased packing order of DOPC resulting from its mixing with SM and Chol. The slight fluctuations at the domain boundary observed after the appearance of oligomers (Figure 1B from 30 s, Movie 1A) might be a consequence of the lateral diffusion of SM and Chol into the DOPC-rich phase. On the basis of these observations, we speculate that the oligomer formation induced the gradual exclusion of SM and Chol from the SM-rich domain by the interruption of SM-SM and SM-Chol interactions, and consequently the lipid mixing. The fluorescence microscopy images support our speculation. The SM/Chol/DOPC (2:1:2) membranes including 1 mol % fluorescent lipid changed significantly after incubating with lysenin (Figure S3). Either a shrinkage in the bright DOPC-rich phase, usually accompanied by unclear phase boundaries, or a homogeneous final morphology was observed. These results indicate that phase mixing occurred, rendering the membrane gel-like or liquid ordered.

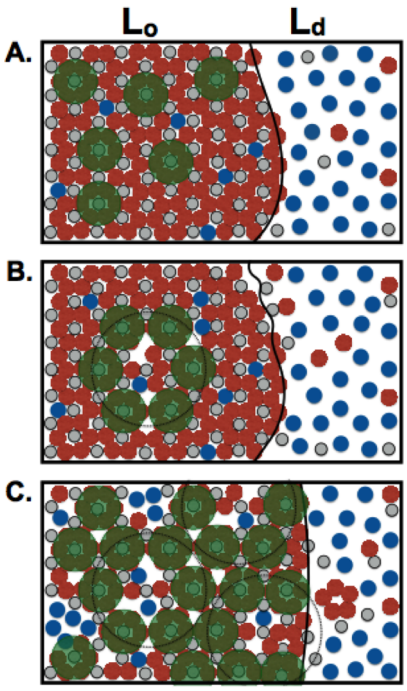

Figure 7. Illustration of the changes in the SM-rich and DOPC-rich phases during assembling of lysenin on the SM-rich domain. The circles filled in red, blue, and gray represent SM, DOPC, and Chol, respectively. Lysenin monomers and oligomers are marked by the green filled circles and the dashed circles, respectively.

We illustrated the SM-rich and DOPC-rich phases during binding of lysenin to SM (Figure 7A) and during the formation of oligomers on the SM-rich domain (Figures 7B,C). Figure 7B shows the exclusion of SM and Chol from the SM-rich domain as a result of oligomer formation. The increasing number of oligomers on the SM-rich domain might lead to the formation of undetectably small SM clusters in the DOPC-rich phase. Such clusters may not be resolved by AFM due to their small size and the presence of Chol, which can render the boundary between SM clusters and the DOPC-rich phase unclear by reducing the line tension.[30] These SM clusters can promote the additional binding of lysenin after the full coverage of the SM-rich domain with oligomers, resulting in the enlargement of the hcp assembly. The slight broadening of the hcp assembly, indicated by the arrow at 300 s in Figure 1B, and the excluded SM in the DOPC-rich phase are depicted in Figure 7C. During the broadening of the hcp assembly we did not observe any lysenin oligomers in the DOPC-rich phase. This might be due to the rapid attraction of the oligomers in the DOPC-rich phase by the hcp assembly through interoligomer interactions. The stable hcp assembly of oligomers surrounding the dynamic DOPC-rich phase (Figure 4) proves the strong interaction between oligomers or SM-bound lysenin. Alternatively, SM-bound lysenin might accumulate in the vicinity of the hcp assembly and oligomerize at the assembly edge. The gradual decrease in the area of the DOPC-rich phase during the continuous formation of oligomers beyond the initial domain boundary (Figure 1B from 240 to 600 s, Figure 2A) indicates the diffusion of DOPC into the hcp assembly. Despite this diffusion, the center-to-center distance between oligomers did not change (Figure 2C). The lysenin oligomers packed with the same neighboring distance in a hexagonal arrangement throughout the entire assembling process. After stabilization of the oligomers, we observed oligomer-free regions marked by the asterisks in Figure 2B. The existence of these defect-like regions within the hcp assembly might be due to the insufficient amount of SM or lysenin. It is likely that some of the DOPC molecules were localized as small domains within the hcp assembly to retain the same packing density of lysenin oligomers instead of entirely mixing with SM and inducing a more disordered arrangement of oligomers. Alternatively, such defects might result from the mismatch between the oligomer arrays, the directions of which are indicated by the black arrows in Figure S4. While the addition of single oligomers to the existing hexagonal assembly may provide a defect-free structure, the binding of small groups of closely packed oligomers may cause imperfections unless they dissociate/reassociate for reorganization.

We investigated the mechanism underlying the exclusion of SM and Chol from the SM-rich domain on the basis of the height analysis. During the membrane reorganization as well as after the hcp assembly of oligomers stabilized, we observed oligomers of different height. The presence of both tall and low oligomers, the heights of which were estimated to be around 11 and 8 nm, respectively, denotes that some of the tall oligomers underwent a conformational change, resulting in their vertical collapse. It is speculated that, in the prepore state the N-terminus of lysenin binds the full length of SM in the outer leaflet of the membrane, although lysenin binds the membrane first through the electrostatic attraction between its C-terminus and the negative charges at the membrane surface.[20] On the basis of this information, an alternative mechanism was suggested.[22] According to this mechanism, lysenin binds SM with the N-terminus tilted upward in the hexameric prepore state. The height of tall oligomers measured during the membrane reorganization agrees with the conformation suggested for the prepore state. In a recent study, the mechanism of prepore to pore transition was revealed for the aerolysin heptamer, which forms a transmembrane β barrel through a swirling movement.[31] Due to the similar structure of lysenin to that of aerolysin,[20,32] we suppose that the vertical collapse in the oligomers of lysenin occurs in a similar way (*i.e.*, by the swirling of N-terminal resulting in the formation of a β barrel and its membrane insertion). The simulations for aerolysin show that the vertical collapse is

around 40% during the transition from prepore to quasi-pore or pore state.[31] Quasi-pore refers to the state at which the formation of the β barrel is not complete. Since the height difference between the tall and low oligomers of lysenin was around 3 nm, indicating a 30% vertical collapse compared to the prepore state, it is likely that the low oligomers of lysenin were either quasi-pores or pores. Thus, lysenin in low oligomers could interrupt the SM−SM and SM−Chol hydrophobic interactions by spanning the membrane partially or fully.

CONCLUSIONS

The results in this work show the full coverage of the initially phase-separated membrane with lysenin oligomers and the pathway followed in the assembling of lysenin. Lysenin first formed oligomers on the SM-rich domain. The phase boundary was almost stable until the SM-rich domain was fully covered by the hcp assembly of lysenin oligomers. The preservation of the phase boundary during the oligomer formation on the SM-rich domain implies that the line tension at the domain boundary could not be reduced by lysenin. Therefore, we attributed the expansion of the hcp assembly into the DOPC-rich phase to the exclusion of SM and Chol from the SM-rich domain. The full coverage of the entire membrane surface by lysenin oligomers denotes the complete mixing of SM-rich and DOPC-rich phases. We tried to reveal the mechanism of phase mixing on the basis of oligomer height. We observed both tall and low oligomers. The height of tall oligomers was consistent with the length of lysenin. Thus, we designated them as prepores. The height difference between the tall and low oligomers indicated that lysenin in prepores underwent a 30% vertical collapse to convert to quasi-pores or pores. The partial or full insertion of lysenin into the membrane possibly led to the interruption of the interactions between lipids in the SM-rich domain and hence the recruitment of SM and Chol into the DOPC-rich phase. It is highly possible that pore formation was needed for phase mixing, which simultaneously increased the number of pores in the membrane and hence elevated the toxin activity.

MATERIALS AND METHODS

Materials. Lysenin from earthworm, *Eisenia fetida*, was obtained from Peptide Institute, Inc. (Osaka, Japan). Egg SM and 1,2-dioleoyl-*sn*-glycero-3-phosphocholine (DOPC) were purchased from Avanti Polar Lipids, Inc. (Alabama, AL). Chol (≥99%) was supplied from Sigma (St. Louis, MO). 1,2-Dioleoyl-*sn*-glycero-3-phosphoethanolamine-*N*-(7-nitro-2-1,3-benzoxadiazol-4-yl) (ammonium salt) (18:1 NBD-PE) and 22-(*N*-(7-nitrobenz-2-oxa-1,3-diazol-4-yl)amino)-23,24-bisnor-5-cholen-3β-ol (22 NBD-Chol) were purchased from Avanti Polar Lipids, Inc. (Alabama, AL) and Invitrogen (Carlsbad, CA), respectively.

Multilamellar vesicles (MLV) of SM/Chol/DOPC (2:1:2) were prepared in a solution of phosphate buffered saline (PBS; 10 mM, pH = 7.5) (Sigma) at a total lipid concentration of 1 mM. Unilamellar vesicles were prepared by sonication of MLVs at 20 kHz with an ultrasonic homogenizer, UH-50 from SMT (Tokyo, Japan), for 10 min. Lysenin was dissolved in PBS to a final concentration of 15 μM.

Visualization of Lysenin Oligomers on Lipid Bilayer. HS-AFM measurements were performed by NANOEXPLORER, developed by Toshio Ando (Kanazawa Univ.) and commercialized by Research Institute of Biomolecule Metrology Co., Ltd. (RIBM; Tsukuba, Japan). The lipid bilayers were prepared by the incubation of 1.5 μL of unilamellar vesicles on a 1.5 mm-diameter mica disk at 55 °C for 15 min. Mica surface was rinsed with Milli-Q water and placed onto the scanner. The surface was imaged in 70−80 μL Milli-Q water or PBS solution with cantilevers having silicon nitride (BL-AC10DS-A2) or carbon nano fiber (BL-AC10FS-A2) probes (Olympus Co.; Tokyo, Japan). Both cantilevers have a spring constant of 0.1 N/m and a resonance frequency in the range between 500 and 600 kHz in water. The scan direction of image acquisition was from left to right. After observation of the fused lipid bilayer, lysenin was introduced into the imaging medium. HS-AFM imaging was performed at room temperature. The analysis of the AFM images was conducted using ImageJ to calculate the area fraction of the DOPC-rich phase and the center-to-center distance between oligomers.

Fluorescence Microscopy Imaging. Fluorescence imaging was performed using Nikon ECLIPSE E600 (Nikon Co.; Tokyo, Japan) equipped with Hamamatsu Digital Camera C11440 (Hamamatsu Photonics KK.; Hamamatsu, Japan). Images were acquired with Nikon CFI Plan Fluor 10× and CFI Plan Fluor 40× objective lenses. The planar lipid membrane was formed on mica surface by vesicle fusion at 55 °C. The membrane was kept hydrated with Milli-Q water or PBS solution. Lysenin was injected into the solution on mica-supported membrane.

Conflict of Interest: The authors declare no competing financial interest.

Acknowledgment. This work was supported by the Integrated Lipidology Program of RIKEN and Grants-in-Aid for Scientific Research 25293015 (to T.K.) from the Ministry of Education, Culture, Sports, Science and Technology of Japan. We thank Dr. Asami Makino for performing GUV experiments with filipin and Dr. Takehiko Inaba for his technical support for the fluorescence microscopy imaging.

Supporting Information Available: The Supporting Information is available free of charge on the ACS Publications website at DOI: 10.1021/acsnano.5b01041.

Movie 1A (AVI)
Movie 1B (AVI)
Movie 2 (AVI)
Movie 3 (AVI)
Movie 4 (AVI)
Movie 5A (AVI)
Movie 5B (AVI)
AFM images showing the stability of the phase boundary before the appearance of lysenin oligomers, the expansion in the membrane area on which the hcp assembly formed, the oligomer dynamics during membrane reorganization, and fluorescence microscopy images showing the change in the membrane after incubation with lysenin. (PDF)

REFERENCES AND NOTES

1. Kobayashi, T.; Stang, E.; Fang, K. S.; de Moerloose, P.; Parton, R. G.; Gruenberg, J. A Lipid Associated with the Antiphospholipid Syndrome Regulates Endosome Structure and Function. *Nature* **1998**, *392*, 193–197.
2. Yeung, T.; Gilbert, G. E.; Shi, J.; Silvius, J.; Kapus, A.; Grinstein, S. Membrane Phosphatidylserine Regulates

Surface Charge and Protein Localization. *Science* **2008**, *319*, 210–213.
3. Lingwood, D.; Simons, K. Lipid Rafts as a Membrane-Organizing Principle. *Science* **2010**, *327*, 46–50.
4. Lee, S.; Uchida, Y.; Wang, J.; Matsudaira, T.; Nakagawa, T.; Kishimoto, T.; Mukai, K.; Inaba, T.; Kobayashi, T.; Molday, R. S.; et al. Transport through Recycling Endosomes Requires EHD1 Recruitment by a Phosphatidylserine Translocase. *EMBO J.* **2015**, *34*, 669–688.
5. de Almeida, R. F.; Fedorov, A.; Prieto, M. Sphingomyelin/Phosphatidylcholine/Cholesterol Phase Diagram: Boundaries and Composition of Lipid Rafts. *Biophys. J.* **2003**, *85*, 2406–2416.
6. Silvius, J. R. Role of Cholesterol in Lipid Raft Formation: Lessons from Lipid Model Systems. *Biochim. Biophys. Acta, Biomembr.* **2003**, *1610*, 174–183.
7. London, E. How Principles of Domain Formation in Model Membranes May Explain Ambiguities Concerning Lipid Raft Formation in Cells. *Biochim. Biophys. Acta, Mol. Cell Res.* **2005**, *1746*, 203–220.
8. Marsh, D. Liquid-Ordered Phases Induced by Cholesterol: A Compendium of Binary Phase Diagrams. *Biochim. Biophys. Acta, Biomembr.* **2010**, *1798*, 688–699.
9. Shaw, J. E.; Epand, R. F.; Sinnathamby, K.; Li, Z.; Bittman, R.; Epand, R. M.; Yip, C. M. Tracking Peptide-Membrane Interactions: Insights from *in Situ* Coupled Confocal-Atomic Force Microscopy Imaging of NAP-22 Peptide Insertion and Assembly. *J. Struct. Biol.* **2006**, *155*, 458–469.
10. Shaw, J. E.; Epand, R. F.; Hsu, J. C. Y.; Mo, G. C. H.; Epand, R. M.; Yip, C. M. Cationic Peptide-Induced Remodelling of Model Membranes: Direct Visualization by *in Situ* Atomic Force Microscopy. *J. Struct. Biol.* **2008**, *162*, 121–138.
11. Garcia-Saez, A. J.; Chiantia, S.; Salgado, J.; Schwille, P. Pore Formation by a Bax-Derived Peptide: Effect on the Line Tension of the Membrane Probed by AFM. *Biophys. J.* **2007**, *93*, 103–112.
12. Ros, U.; Edwards, M. A.; Epand, R. F.; Lanio, M. E.; Schreier, S.; Yip, C. M.; Alvarez, C.; Epand, R. M. The Sticholysin Family of Pore-Forming Toxins Induces the Mixing of Lipids in Membrane Domains. *Biochim. Biophys. Acta, Biomembr.* **2013**, *1828*, 2757–2762.
13. Rojko, N.; Cronin, B.; Danial, J. S. H.; Baker, M. A. B.; Anderluh, G.; Wallace, M. I. Imaging the Lipid-Phase Dependent Pore Formation of Equinatoxin II in Droplet Interface Bilayers. *Biophys. J.* **2014**, *106*, 1630–1636.
14. Athanasiadis, A.; Anderluh, G.; Macek, P.; Turk, D. Crystal Structure of the Soluble Form of Equinatoxin II, a Pore-Forming Toxin from the Sea Anemone. *Structure* **2001**, *9*, 341–346.
15. Mancheno, J. M.; Martin-Benito, J.; Martinez-Ripoll, M.; Gavilanes, J. G.; Hermoso, J. A. Crystal and Electron Microscopy Structures of Sticholysin II Actinoporin Reveal Insights into the Mechanism of Membrane Pore Formation. *Structure* **2003**, *11*, 1319–1328.
16. Črnigoj Kristan, K.; Viero, G.; Dalla Serra, M.; Macek, P.; Anderluh, G. Molecular Mechanism of Pore Formation by Actinoporins. *Toxicon* **2009**, *54*, 1125–1134.
17. Makino, A.; Abe, M.; Murate, M.; Inaba, T.; Yilmaz, N.; Hullin-Matsuda, F.; Kishimoto, T.; Schieber, N. L.; Taguchi, T.; Arai, H.; et al. Visualization of the Heterogeneous Membrane Distribution of Sphingomyelin Associated with Cytokinesis, Cell Polarity, and Sphingolipidosis. *FASEB J.* **2015**, *29*, 477–493.
18. Yamaji, A.; Sekizawa, Y.; Emoto, K.; Sakuraba, H.; Inoue, K.; Kobayashi, H.; Umeda, M. Lysenin, a Novel Sphingomyelin-Specific Binding Protein. *J. Biol. Chem.* **1998**, *273*, 5300–5306.
19. Yamaji-Hasegawa, A.; Makino, A.; Baba, T.; Senoh, Y.; Kimura-Suda, H.; Sato, S. B.; Terada, N.; Ohno, S.; Kiyokawa, E.; Umeda, M.; Kobayashi, T. Oligomerization and Pore Formation of a Sphingomyelin-Specific Toxin, Lysenin. *J. Biol. Chem.* **2003**, *278*, 22762–22770.
20. De Colibus, L.; Sonnen, A. F.-P.; Morris, K. J.; Siebert, C. A.; Abrusci, P.; Plitzko, J.; Hodnik, V.; Leippe, M.; Volpi, E.; Anderluh, G.; Gilbert, R. J. C. Structures of Lysenin Reveal a Shared Evolutionary Origin for Pore-Forming Proteins and Its Mode of Sphingomyelin Recognition. *Structure* **2012**, *20*, 1498–1507.
21. Ishitsuka, R.; Yamaji-Hasegawa, A.; Makino, A.; Hirabayashi, Y.; Kobayashi, T. A lipid-Specific Toxin Reveals Heterogeneity of Sphingomyelin-Containing Membranes. *Biophys. J.* **2004**, *86*, 296–307.
22. Yilmaz, N.; Yamada, T.; Greimel, P.; Uchihashi, T.; Ando, T.; Kobayashi, T. Real-Time Visualization of Assembling of a Sphingomyelin-Specific Toxin on Planar Lipid Membranes. *Biophys. J.* **2013**, *105*, 1397–1405.
23. Quinn, P. J.; Wolf, C. Egg-Sphingomyelin and Cholesterol Form a Stoichiometric Molecular Complex in Bilayers of Egg-Phosphatidylcholine. *J. Phys. Chem. B* **2010**, *114*, 15536–15545.
24. Samsonov, A. V.; Mihalyov, I.; Cohen, F. S. Characterization of Cholesterol-Sphingomyelin Domains and Their Dynamics in Bilayer Membranes. *Biophys. J.* **2001**, *81*, 1486–1500.
25. Goni, F. M.; Alonso, A.; Bagatolli, L. A.; Brown, R. E.; Marsh, D.; Prieto, M.; Thewalt, J. L. Phase Diagrams of Lipid Mixtures Relevant to the Study of Membrane Rafts. *Biochim. Biophys. Acta, Mol. Cell Biol. Lipids* **2008**, *1781*, 665–684.
26. Puech, P.-H.; Borghi, N.; Karatekin, E.; Brochard-Wyart, F. Line Thermodynamics: Adsorption at a Membrane Edge. *Phys. Rev. Lett.* **2003**, *90*, 128304.
27. Hutchison, J. B.; Weis, R. M.; Dinsmore, A. D. Change of Line Tension in Phase-Separated Vesicles upon Protein Binding. *Langmuir* **2012**, *28*, 5176–5181.
28. Lis, L. J.; Mcalister, M.; Fuller, N.; Rand, R. P.; Parsegian, V. A. Measurement of the Lateral Compressibility of Several Phospholipid Bilayers. *Biophys. J.* **1982**, *37*, 667–672.
29. Bonn, M.; Roke, S.; Berg, O.; Juurlink, L. B. F.; Stamouli, A.; Müller, M. A Molecular View of Cholesterol-Induced Condensation in a Lipid Monolayer. *J. Phys. Chem. B* **2004**, *108*, 19083–19085.
30. Pandit, S. A.; Jakobsson, E.; Scott, H. L. Simulation of the Early Stages of Nano-Domain Formation in Mixed Bilayers of Sphingomyelin, Cholesterol, and Dioleylphosphatidylcholine. *Biophys. J.* **2004**, *87*, 3312–3322.
31. Degiacomi, M. T.; Iacovache, I.; Pernot, L.; Chami, M.; Kudryashev, M.; Stahlberg, H.; van der Goot, F. G.; Peraro, M. D. Molecular Assembly of the Aerolysin Pore Reveals a Swirling Membrane-Insertion Mechanism. *Nat. Chem. Biol.* **2013**, *9*, 623–629.
32. Szczesny, P.; Iacovache, I.; Muszewska, A.; Ginalski, K.; van der Goot, F. G.; Grynberg, M. Extending the Aerolysin Family: from Bacteria to Vertebrates. *PLoS One* **2011**, *6*, e20349.